of atmospheric water collection apparatuses. Particularly, it pertains to an air-borne water harvesting system that operates through adsorption. Typically, water is procured during chilling nocturnal periods with heightened RH, subsequently desorbing during daytime as temperatures rise. Preferably, the energy necessitated for desorption is harnessed from solar radiation, obviating the necessity for supplementary energy input. Xin et al. fabricated a poly(*n*-isopropylacrylamide) sponge-like cotton fabric featuring temperature-responsive wettability alterations, capable of autonomously accumulating and discharging moisture from humid air. Microscopically, temperature fluctuations instigate structural transformations in thermoresponsive polymers, synergistically with augmented surface texture, allowing sponge-like material to reversibly alternate between superhydrophobic and superhydrophilic states [43]. This permits water to be harvested during nocturnal hours, followed by water desorption during daytime temperature ascension. Subsequently, investigators concentrated on devising alternative absorbent materials from a viewpoint of reduced energy expenditure and facile processing [44], encompassing hydrogels, three-dimensional porous structures [45], fabrics, nanoscale powders [46], and silica fibers [47]. For instance, Kim et al. synthesized a Ni-IRMOF74-III metal–organic framework architecture, which is adorned with azopyridine molecules. This MOF can undergo photochemically triggered cis/trans transitions, demonstrating superior water collection proficiency compared to other MOF-based water collectors, even under minimal temperature oscillation conditions.

Hydrogels, owing to their high hydrophilic nature and remarkable water retention capacity, are emerging as promising water collection and storage materials [48]. For instance, Wang et al. have devised a flexible hybrid light-thermal adsorbent comprising deliquescent salt and hydrogel, competent of capturing fog in the atmosphere [49]. Distinct from other hydrogels, this salt gel incorporates hygroscopic, nontoxic, environmentally friendly $CaCl_2$, preserving outstanding water absorption capacity even in low humidity settings. Due to the incorporation of hydrogel structure, the saltwater gel retains its solid form after substantial water absorption. The saltwater gel further incorporates carbon nanotubes and displays typical photothermal effects, swiftly discharging water upon routine sunlight exposure. With a judicious material design, the hydrogel can accumulate and discharge water intermittently at dusk and dawn.

Currently, atmospheric water collection systems employing adsorbent methods perform a unique daily water collection cycle, yet freshwater procured through this methodology still markedly lags behind in meeting escalating potable water requirements. Despite endeavors to implement techniques that curtail the adsorption–desorption cycle, collection efficacy remains restricted by the protracted cycle duration. Additionally, the absorbed water must be discharged in sunny conditions, thus impeding the ultimate production of fresh water on cloudy days. In addition, given climatic discrepancies across various nations and regions, and climate fluctuations across seasons, the adsorbent water harvesting capacity may be significantly reduced or even rendered ineffective. Hence, it is imperative to consider the potential impact of these objective factors during the material design and fabrication process. In arid regions, where the water absorption capacity of materials diminishes in low humidity environments, the water collection

performance of most water collection materials is substandard. Consequently, researchers are innovating novel composite materials to permit their utilization in low humidity conditions, such as encapsulating hygroscopic salts within the adsorbent matrix [50].

1.3 Biomimetic Inspiration for Collecting Fog

The Namibian Desert, located within Africa, is recognized as one of the earliest and driest global deserts, serving also as the single coastal desert globally. Consequently, this desert presents a massive terrain of sand dunes influenced by fog. The ocean fog constitutes a primary source of nourishment for the vegetation, snakes, spiders, beetles, and lizards that inhabit this area. Over millennia of evolution, numerous creatures have adapted diverse tactics to survive while utilizing fog. For instance, Parker and Lawrence documented a fog collection strategy employed by the Namibian desert beetle Stenocara [27]. Studies indicate that the hydrophobic wax layer solely envelops the elevated regions of the insect's exoskeleton. Conversely, these elevated sites (ranging in diameter from 0.5 to 1.5 mm and positioned at intervals of 0.5–1.5 mm) lack the wax layer, demonstrating hydrophilic characteristics. It is postulated that this alternation between hydrophobicity and hydrophilicity contributes significantly to the beetle's proficient fog collection capability. The hydrophilic regions on its back efficiently trap minute droplets, facilitating their swift coalescence into larger ones. With sufficient aggregation, the large droplets exploit the hydrophobic nature of the adjacent region to swiftly roll toward the head where they are gathered and utilized. Motivated by this distinctive architecture of alternating hydrophilic projections and hydrophobic surroundings, several biomimetic materials have been engineered and exhibit superior fog collection abilities. Among them, superhydrophobic/superhydrophilic patterned surfaces with micro/nanoscale textures have been successfully produced through physical and chemical methodologies, resulting in a relatively advanced fabrication technique. The principal techniques encompass five categories: photolithography [51], mechanical micromilling [52], composite technology employing distinct wettability materials [53], stimulus-responsive fog capture technology [54], and inkjet printing technology [55] (Figure 1.4).

In the production of water fog collectors using artificial desert beetle scales as a model, we primarily manipulate surface wettability and devise patterned surfaces to influence collection efficiency. In controlling surface wettability, we utilize selective chemical hydrophobic modifications, regulating the content of iron and cobalt particles on fiber fabrics to generate surfaces with varying degrees of hydrophobicity. Our experiments demonstrated that escalating the proportion of hydrophobic particles shortens the duration of the first drop of water rolling off the fiber surface. Conversely, augmenting hydrophilic particles prolongs this time. These superhydrophobic–superhydrophilic surfaces offer cost-effective and convenient advantages, but the distribution of hydrophobic and hydrophilic particles is disordered. We discovered in subsequent studies that the arrangement pattern of different hydrophilic and hydrophobic patterns significantly impacts water fog

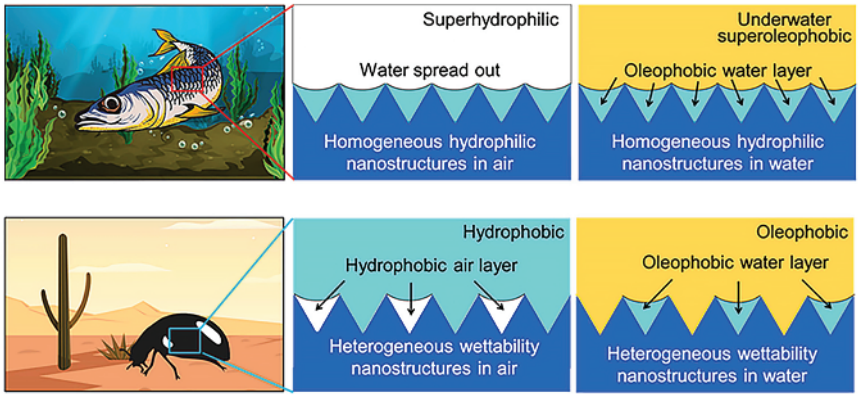

Figure 1.4 Surface wettability of fish scales and surface wettability of desert beetles. Source: [56] / American Chemical Society.

collection [57]. Indeed, from a morphological perspective, the differences between fabricated bionic surfaces are significant at the micro/nanoscale, but negligible at the macroscopic scale. The presence of hydrophilic regions primarily facilitates the rapid capture of liquid droplets. After experiencing the water fog supply phase, larger droplets can rapidly detach for the hydrophilic region to initiate another round of water fog capture. Therefore, it is crucial to investigate whether geometric structure design can expedite droplet detachment to strategically enhance water fog collection efficiency. We compared the process of water fog collection on two patterned surfaces: hemispherical hydrophilic projections and linear hydrophilic projections. It was found that over the same period, droplets could be captured more quickly and aggregated into a critical size on the surface arranged linearly. Moreover, the anisotropy of linear projections results in droplets picking up more droplets along their descent path, hence exhibiting superior water fog efficiency. Furthermore, considering the fluid characteristics of the water fog, diverse surface geometries will interfere with the movement of droplets in the fog. For instance, Aizenberg et al. observed in their study of condensation of water vapor on wet slippery projections that discontinuities in the surface can amplify the diffusion flux of water vapor, thereby enhancing the water supply rate. Thus, the impact of the geometric morphology of bionic surfaces on the overall water fog collection should not be overlooked, particularly its effect on the water fog supply process warrants further research. To this end, we produced a series of superhydrophobic projections with varying arrangements and quantities, revealing distinct effects on the enhancement of droplet growth rates. Using Fluent software, computational fluid dynamics (CFD) clearly illustrated that these projections can modify the dynamic pressure distribution over the surface and concentrate fluid (composed of microdroplets and air) around the projection. Droplets surrounding the projection exhibit higher velocity than those adjacent to the plane, thus these high-energy droplets can be captured more quickly by the projection surface. Consequently, these projections capture more microdroplets, and the growth speed of droplets

on them can be substantially accelerated. The various patterned surfaces of the artificial desert beetle rely on gravity to induce droplet detachment. So how can we optimize the water transport process and improve water fog collection efficiency? The following sections will provide additional inspiration and strategies from spider silk and cacti, where the driving force can also be provided by surface energy gradients and Laplace pressure. How to optimize the design of three fundamental processes to realize an efficient water fog collection system has been our ongoing endeavor in both the past and present.

In 2010, Zheng and coworkers unveiled the concept of spider silk fog collection for the first time. They observed that under moist conditions, spider silk fabricates a structure consisting of alternating coarse conical spindle knots and fine junction points. This distinctive structure plays an integral role in directed water collection [58]. The spindle knot region is formed by highly randomized nanofibers, exhibiting high roughness; conversely, the junction region comprises orderly nanofibers arranged with lower roughness. Moreover, each repeating unit comprising spindle knots and junction points can be viewed as a spindly structure whose diameter varies gradually. Hence, spider silk in humid environments possesses unique surface energy and geometric structure gradients, which serve as driving forces for directional droplet transport. The surface energy gradient prompts droplets to move from the junction to the more hydrophilic spindle knot, while the geometric structure gradient generates a Laplace pressure difference, propelling droplets from the junction (high curvature area) to the conical spindle knot (low curvature area). Consequently, the mystery behind the efficient, continuous process of spider silk capturing, condensing, transporting, and accumulating fog has been unraveled, offering novel strategies for scientists to develop biomimetic fog collectors.

Undeniably, the size and surface morphology of artificial spindle knots, the spacing between spindle knots, etc., significantly affect the efficiency of fog collection when mimicking spider silk. For instance, Zheng et al. fabricated heterogeneous spindle knot microfibers using electrospinning. This technique effectively modulates the morphology of spindle knots by altering the concentration of calcium chloride in the fluid [58]. Experiments show that the morphology of spindle knots directly impacts the efficiency of fog collection. Greater roughness implies a higher gradient of surface energy, resulting in superior fog collection efficiency. Furthermore, this technology allows precise control of the distance between spindle knots and junction points by adjusting the flow rate. They discovered that when the interval between two spindle knots increases, it becomes challenging for droplets on adjacent spindle knots to coalesce, leading to prolonged maximum droplet formation time, extended water collection period, and reduced water collection efficiency. In addition, factors influencing the critical droplet detachment volume were examined, revealing that the geometry of the prepared spider silk fiber significantly influences the size of suspended droplets [59]. This is attributed to the hump (spindle knot), which enhances the stability of the triple phase contact line through the combined effects of slope and curvature, thereby providing sufficient capillary adhesion for suspended droplets. Therefore, incorporating small-sized spindle knots between two larger spindle knots into multi-scale, multi-gradient

biomimetic fibers was proven to be an effective strategy to enhance the fiber's ability to suspend droplets and achieve higher water collection efficiency [60].

The cactus can be seen as a sophisticated combination of architecture and functionality within a dew collection system. Its spines, composed of three distinct structural features, namely, pointed barbs at the tip, gradient grooves in the middle, and banded hairlike structures at the base, synergistically facilitate the capture and directional transportation of droplets. Like spider silk's mechanism for fog collection and transport, the initial droplet is captured and grows simultaneously on both the barb and the main stem of the spine. Subsequently, the large droplet on the barb migrates toward the root of the barb and merges with the droplet on the main stem. Given that the entire spine is a tapered geometric structure, there exists a difference in the Laplace pressure from the apex to the root. Moreover, the spine is adorned with a hydrophobic plant wax layer, and the groove presents an anisotropic distribution; the density of the spine tip is higher than that of the root, thus creating a gradient of surface energy between the tip and the root of the spine. Consequently, as the barb and main stem of the spine continue to capture and merge droplets, the merged large droplet commences its journey to the root under the combined influence of the Laplace pressure difference and the surface energy gradient. It is also noteworthy that this collection mechanism involves the rapid absorption of droplets upon contact with the hairlike structures of the spine root as most current dew collection systems incorporate an open collection vessel, which inevitably leads to some water evaporation loss.

Inspired by the cactus's dew collection mechanism, focusing on droplet capture and removal (transportation), the fabrication of tapered collection spines with dual gradients of structure and wettability can enhance the self-propulsion of captured droplets and expedite the regeneration of collection sites under the dual gradients of surface energy and structure. We achieved this by a precipitation post modification method, where a gradient change in wetting properties was obtained from the hydrophobic apex to the hydrophilic root of the modified superhydrophobic copper needle by gradient deposition of hydrophilic micronanoparticles on the substrate. When a droplet encounters a surface with a gradient of structure and wettability, it can undergo antigravity transportation despite being in a negative angle state, propelled by the driving force of the gradient of structure and surface energy. Thanks to the efficient transportation of droplets, this dew collection device can rapidly regenerate the dew collection surface and accelerate the dew collection cycle, thereby demonstrating outstanding dew collection performance [61]. Liu and coworkers, by mimicking the cactus's tapered spine structure, fabricated a flexible magnetic responsive spine array to improve the capture and collection ability of fog droplets in low-fog flow rate environments [62]. Under the action of an external magnetic field, the likelihood of collision between the oscillating spine and the fog droplet increases, and due to the periodic oscillation of the tapered spine, the effective dew collection area of the spine is expanded. Therefore, the magnetically controlled flexible tapered spine array exhibits excellent dew collection capability in low fog flow environments, while in the same scenario, due to the lower fog speed, fog is difficult to capture without an external magnetic field, and fog collection efficiency can

be negligible. The design of the flexible tapered spine shows that researchers have taken account of the impact of fog flow rate during the dew collection process on the efficiency of dew collection, and they are also paying attention to the double aspects of the fog capture process and the transport link.

Inspired by the strikingly diverse water droplet capture, condensation and transport systems exhibited by the Namib Desert beetle, spider silk, and cactus, we engineered multifunctional patterned surfaces, heterostructured fibrous threads, and conical needle prongs for efficient water collection. The synergistic interplay between structural gradients and surface energy gradients enables rapid droplet removal; however, beyond droplet removal, capturing, condensing, and mitigating evaporation before reaching the critical droplet detachment (transportation) volume are crucial considerations in achieving high-efficiency water collection. Integrating a single or dual specific water collection mechanism is insufficient to achieve an integrated, multifunctional water droplet capture, condensation, transportation, and collection process. Therefore, designing novel multifunctional superwetting devices or systems and establishing theoretical models to analyze the influence mechanisms of surface topography and wettability, and geometry on water droplet collection are areas that require our attention and effort. Through relentless exploration in the field of water droplet collection, several bioinspired, multifunctional water droplet collection systems have been reported, demonstrating an efficient cycle of droplet capture, condensation, and transport during the collection process. Lai and coworkers summarized the evolution of water droplet collection devices from single biomimicry to multiple biomimicry, suggesting that more organisms with efficient collection mechanisms may be discovered in the future [63]. At present, multiple biomimetic devices can be classified as double biomimicry, triple biomimicry, and even quadruple biomimicry. How to skillfully integrate the mechanisms of water droplet collection from different animals and plants and consider the three fundamental processes of water droplet collection fully embodies the cutting-edge development of the field of water droplet collection. In this section, we will briefly introduce the design concepts of several typical multiple biomimetic water droplet collection systems, aiming to provide readers with a basic understanding of the integrated design and advanced development of water droplet collection systems.

The upper and lower surfaces of lotus exhibit complete wettability, with the upper surface exhibiting superhydrophobicity and the lower surface exhibiting superhydrophilicity. Inspired by the asymmetric wetting properties of lotus leaves, a series of Janus materials with asymmetric wetting properties were designed and fabricated. For Janus materials, the asymmetric wetting properties on both sides generate a wetting driving force on droplets, causing them to transport unidirectionally from the hydrophobic side to the hydrophilic side but not in reverse. During the water droplet collection process, Janus materials can accelerate the unidirectional penetration and removal of captured droplets, improving the problem of slow regeneration of capture sites due to gravity-induced droplet shedding and large droplet evaporation losses. As a result, many teams have strategically incorporated Janus materials into a water droplet collection system along with

other biomimetic devices to achieve higher water droplet collection efficiency than surfaces with homogeneous wetting properties. For example, by combining Janus materials with the hydrophilic–hydrophobic wetting characteristics of desert beetles, we successfully prepared hydrophilic–hydrophobic/superhydrophilic copper foam through hydrothermal growth and local modification [64]. This Janus copper foam balances the three basic water droplet collection processes. The hydrophilic–hydrophobic surface facilitates the capture and condensation growth of water droplets, while the asymmetric wetting property further promotes the transport and removal of water droplets. Therefore, compared to homogenous wetting copper foam mainly relying on gravity-induced droplet removal, Janus foam copper exhibits superior water droplet collection performance. Similarly, integrating the tapered structure of cacti and Janus properties is also a design approach for a water droplet collection device [65].

The utilization of fluid-percolation surfaces in achieving low contact angle hysteresis and rapid droplet motion, benefiting from their ability to regenerate nucleation sites and enhance condensing heat transfer, has become a promising strategy for designing efficient fog collection systems. For example, we have successfully engineered an interdisciplinary four-dimensional bioinspired fog collection system by blending features from the bumpy structure and wettability distribution of desert beetles, conical structures of cactus spines, seed propulsion behavior of aquatic plants, and slippery surfaces of pitcher plants [66]. This multifunctional fog collection system is composed of superhydrophilic copper needles and regular hydrophilic bumps, with a zinc sheet substrate surrounding a hydrophobic slip surface. The top of the bump features regular circular holes, into which the superhydrophilic copper needle is inserted vertically and anchored to a sponge base. Numerous droplets captured by the slip surface are swiftly transported to the top of the bump due to the oil meniscus effect generated by the bump, significantly enhancing droplet transportation and regeneration of nucleation sites. Similar to the movement of seeds toward aquatic vegetation, the oil meniscus around the hydrophilic bump on the hydrophobic slip surface exerts capillary driving force on the droplets, causing them to move toward the bump in all directions. The structural gradient and superhydrophilicity of the tapered copper needle can help address the issue of hindering droplet removal due to the formation of a water film on the hydrophilic buffer, thereby minimizing the time required for water collection circulation. Therefore, this multifunctional bioinspired fog collection system not only facilitates droplet capture, unidirectional pumping, but also accelerates droplet removal and storage, demonstrating the comprehensive and coordinated nature of the three fundamental processes involved in fog collection.

It is worth noting that during the design and development of fog collection systems, considerable research attention has been paid to a crucial factor influencing fog collection – the velocity of the fog flow reaching the fog capture surface. When discussing the bioinspired fog collection concept using nanoscale cloth desert beetles, we observed how the geometry of the surface bumps could influence the flow distribution of the fog fluid, further impacting the supply of fog during the collection process. Thus, for two-dimensional fog collection surfaces, hydrophilic

bumps and hydrophobic surrounding patterns are generally recognized as having enhanced fog collection capabilities. However, our findings reveal that compared to the impact of surface wettability, the diameter of one-dimensional copper wires has a more significant impact on fog collection efficiency [67]. In other words, it is imperative to recognize that when one-dimensional and two-dimensional materials are placed within the fog flow, they induce distinct levels of interference in the fog flow. While air flows over a two-dimensional plane, substantial entrainment occurs; however, for one-dimensional linear materials, this deviation is significantly reduced, resulting in higher energy fog droplets being captured by the surface. Therefore, the fog collection capacity of superhydrophobic copper wires, superhydrophilic copper wires, pristine copper wires, and copper wires with alternating hydrophilic and hydrophobic regions exhibits minimal differences. From these observations, it becomes evident that when designing fog collection devices, it is essential to consciously consider factors such as fog flow interference, for example, when designing tapered arrays on a two-dimensional plane, considering how the arrangement (square or hexagonal) of the array affects fog flow interference [68].

The above delineation succinctly prescribes biomimetic approaches in fog collection. The detailed design and fabrication of specialized fog collectors or systems will be thoroughly examined and introduced in subsequent chapters of this enlightening book. Subsequently, we will elaborate the supporting theories of fog collection from three interrelated dimensions: the surface nucleation mechanism of water molecules, the growth theory of surface droplets, and the fundamental principles of surface transport behavior. Currently, the design of fog collection systems is transitioning from a singular biomimicry approach to a multifaceted one. In the future, it is expected that more ingenious fog collection strategies derived from flora and fauna will be seamlessly integrated into these devices. On the basis of the currently recognized three fundamental processes of fog collection, there is an urgent need to establish more comprehensive theoretical models to analyze the influence of surface geometry and wettability on fog collection, thereby fostering a feedback loop between theory and practice for potential practical implications in the design and application of fog collection systems.

1.4 Biomimetic Fog Collection Performance Evaluation

While a variety of techniques exist for harvesting atmospheric water, it is challenging to compare them under uniform standards. The challenges are multifaceted. First, fog and dew collection are impacted by climatic conditions as well as location factors, with fog collection necessitating higher humidity environments than those suitable for adsorption-based atmospheric water collection. This implies that through research on diverse water collection methodologies, we must select appropriate collection methods in varying regions and environments to achieve site-specific benefits. Consequently, an evaluation of the performance of atmospheric water collection without regard to applicable environmental parameters is meaningless. Second, fog water collection ensues when minute droplets in

the atmosphere collide with the surface of a fog collector and are subsequently captured and collected. There is no phase change involved in this process, nor does it require input of energy; it is a passive method of collection. For fog water collection, the momentum provided by airflow, the size and density of fog droplets, etc., are critical environmental factors influencing its efficiency. On the other hand, both dew collection and adsorption-based atmospheric water collection involve phase changes. These two types of atmospheric water collection can be classified according to whether external energy is required or not into cooling-based atmospheric water collection and adsorption-based atmospheric water collection, respectively. Therefore, for active collection requiring energy input, assessing its collection efficacy necessitates consideration of both the collection rate and energy consumption. Henceforth, we will succinctly analyze which environmental factors are pivotal determinants of the performance of various water collection technologies using the evaluation metrics currently employed, with the aim of providing a benchmark for test environments in evaluating atmospheric water collection, enabling a more informed comparison of the performance of similar water collection technologies.

In Wang et al.'s summary of progress in atmospheric water collection, they mention three metrics typically utilized to evaluate atmospheric water collectors – specific water production (SWP) per day per unit collector area, specific energy consumption (SEC) per unit mass water production, and feed air recovery ratio (RR). SWP is generally used to assess the water production capacity of passive atmospheric water collectors (which do not require energy input), while SWP and RR are more frequently applied to evaluate the energy efficiency and water vapor condensation effect of active atmospheric water collectors. For direct cooling water collection, SEC and RR are defined as follows:

$$\mathrm{SEC} = \frac{Q_{\mathrm{cond}}}{m_{\mathrm{H_2O}}} \approx C_p \left(\frac{\varepsilon_T}{\varepsilon_d}\right)\left(\frac{T_{\mathrm{i}} - T_{\mathrm{cond}}}{d_{\mathrm{i}} - d_{\mathrm{cond}}}\right) + h_{\mathrm{fg}}, \tag{1.6}$$

$$\mathrm{RR} = \varepsilon_d \left(1 - \frac{d_{\mathrm{cond}}}{d_{\mathrm{i}}}\right). \tag{1.7}$$

In the formulation, T_{i} signifies the temperature of the inlet airstream in the condenser and d_{i} indicates its humidity ratio. T_{cond} denotes the condensing temperature. This indicator measures the water production rate per unit mass of dry air (kilograms per kilogram). The parameters ε_{T} and ε_{d} signify the heat transfer and mass exchange efficiencies of the condenser, respectively. The total cooling load Q_{cond} of moist air encompasses both sensible heat load associated with the temperature change of wet air and latent heat load related to the condensing enthalpy (h_{fg}). Evidently, a lower sensible heat load may result in a smaller SEC, implying that inlet air necessitates a higher RH. SEC and RR definitions suggest that an optimal inlet air condition exists with low T_{cond}, low T_{i}, and high d_{i}. Similarly, Broday et al.'s moisture harvesting index (MHI) , which has gained widespread acceptance as a metric for quantifying the energy required for dew collection [69], although it does not quantify the actual system's energy consumption, considers the ratio between the minimum

energy requirement for condensation and the specific energy and latent heat of each unit mass of water at a given inlet air condition [10]. MHI is defined as

$$\mathrm{MHI} = h_{\mathrm{fg}}/q. \tag{1.8}$$

In this context, $q = (h_{\mathrm{o}} - h_{\mathrm{i}})/(r_{\mathrm{o}} - r_{\mathrm{i}})$, where h_{o} and h_{i} mean the enthalpy in air at the outlet and inlet states, respectively, while r_{o} and r_{i} represent the humidity ratio (kg water per kg air) of these respective conditions [70]. The maximum value for MHI is 1, corresponding to pure saturated steam. Conventionally, the exhaust state of the damper system is set at a temperature of 4° C, with a humidity ratio of 5 g water per kg air. When MHI falls below zero, it means that either the inlet temperature or humidity is below the assumed outlet condition. A higher MHI generally facilitates dew formation, indicating reduced latent cooling demand and increased water production from incoming air [10]. MHI < 0.3 is considered highly impractical for dew collection conditions, even when using advanced dew systems under standard operating conditions [70]. Bagheri has tested commercial dew systems under various environmental conditions, yielding results consistent with predictions; the SEC of the dew system is highly dependent on ambient humidity and temperature [69]. SEC can be linked to MHI through a simple relationship: SEC × MHI = H_{fg}[12]. Based on the above analysis, the key environmental factors influencing the performance of atmospheric water collection based on cooling are humidity and temperature. Currently, the water yield ratio used to express dew collection is typically expressed as kg per day (active cooler) or kg m^{-2} day (passive radiative cooler). For atmospheric water collection based on adsorption, equilibrium vapor absorption in materials (water absorption per kilogram dry adsorbent, kg kg^{-1}) identified from adsorption isotherms is often used as an indicator of water collection water yield.

In fact, fog collection currently uses a single SWP as its evaluation metric. Commercial humidifiers are frequently used in laboratory simulations of foggy environments to evaluate the performance of biomimetic fog collectors. Generally, parameters such as temperature, RH, fog flow rate (cm s^{-1}), fog flux (mg s^{-1}), sample tilt angle, and distance between the sample and humidifier (x) can be controlled. How these parameters affect fog collection performance and how the reasonableness of parameter settings is determined can be measured by examining the collection environments of organisms and plants capable of collecting fog in nature. After Parker et al. discovered the fog collection capacity of desert beetles, they simulated the collection environment of desert beetles (desert wind speed of 5 m s^{-1}, tilt angle of 45°), utilizing Euler's first law. At this V wind speed, droplets roll down,

$$V = \sqrt{\left(\frac{4\rho_{\mathrm{water}}}{3\rho_{\mathrm{air}}} Rg\sin\theta\right)}. \tag{1.9}$$

Here, R is the droplet radius, g is the gravitational constant (9.8 m s^{-2}), θ is the tilt angle, and ρ is the medium's density ($\rho_{\mathrm{air}} = 1\,\mathrm{kg\,m^{-3}}$, $\rho_{\mathrm{water}} = 1000\,\mathrm{kg\,m^{-3}}$).

In this experimental setting, a spherical droplet must exceed a diameter of 5 mm to roll down. The desert beetle observed in actual conditions has droplets rolling off its back with diameters between 4 and 5 mm, validating the simulation results. Consequently, it is evident that wind speed equivalent to fog flow rate influences the size of droplets relying on gravity for descent, thereby affecting the efficiency of fog collection. Moreover, a specific fog flow rate also affects the kinetic energy imparted by airflow to droplets reaching the surface of the fog collector. Only sufficient kinetic energy can allow droplets to collide with the collector surface and be captured. As the airflow transports the droplets closer to the collector surface, some of the kinetic energy will be converted into viscous loss energy W due to friction resistance. According to Chandra et al.'s work, the viscous loss can be estimated as [71]

$$W \sim \varphi V t_c. \tag{1.10}$$

Here, V is the volume of fog droplets, and φ is a loss function, given by the following equation:

$$\varphi \sim \mu(U/r)^2. \tag{1.11}$$

Substituting into our equation, one observes that μ denotes the fluid's dynamic viscosity and U exemplifies the droplet's speed, while r signifies the radius of the droplet. Now, let us designate t_c, or time for complete coalescence, as the time required for a droplet to experience its utmost deformation postimpact with a rigid boundary at velocity U. We opt for the peak value,

$$t_c \sim r/U. \tag{1.12}$$

In addition, the kinetic energy of fog droplets is

$$\Delta E_k = 0.5\, mU^2. \tag{1.13}$$

In this context, m pertains to the mass of the fog droplet. Pertaining to the capture process, it is necessary for the system to surmount an energy barrier known as E in order to secure the attachment of fog droplets to the surface of a fog collector. From the energy point of view during the capture period, it becomes imperative that the fog droplet can be successfully captured by the material surface if the following relationship is confirmed: $E_k > E + W$. Basically, the fog droplet requires additional energy beyond the viscous loss during collision to be effectively captured on the surface of the fog collector.

Specifically, the fog flow degrades when fog droplets deviate from the material surface, thereby significantly reducing their kinetic energy; at such times, the impact of the fog flow rate on collection effectiveness also comes into play. Boundary layer theory can be used to describe the velocity gradient formed before fog droplets reach the catcher's surface during dynamic fog capture [72]. When fog droplets encounter the object's surface, there exists a velocity gradient along the vertical direction of the surface, which is referred to as the boundary layer [63]. The speed of the fog droplet will be influenced by the boundary layer upon impact on the object. The thickness of the boundary layer shows a negative correlation with the flow rate of fog. The speed U

of the fog droplet in the fog stream can be considered equivalent to the air current speed (70 cm s^{-1}). The Reynolds number (*Re*) is expressed as

$$Re = \frac{\rho U d}{\mu'}. \tag{1.14}$$

In this context, ρ and μ' represent the density and viscosity of the fog stream, respectively. The standard length, d, of a flat, smooth plate can be defined as unity. The calculated Reynolds number (roughly equivalent to 5×10^4) is lower than the standard value (5×10^5), indicating that the fog stream may be considered laminar. For laminar flows, the plate boundary layer thickness (δ) can be determined using the following equation:

$$\delta = 5xRe^{-0.5}. \tag{1.15}$$

In such experiments, x represents the distance between the fog collector and the fog flow (normally 0 to 20 mm). As shown in Eq. (1.15), the calculated δ is below 45 μm, indicating a significant deceleration of droplets as they pass through the fog collection zone. The droplet's reduced velocity results in fewer collisions with the substrate per unit time, making it challenging for kinetic energy to be completely exhausted. On surfaces with protuberances, droplets exhibit higher velocities on surfaces with an uneven, thin boundary layer structure, which escalates the frequency of droplet–substrate collisions, rapidly depleting the kinetic energy of droplets, thereby achieving superior fog collection efficiency.

In addition, the RH and fog flow rate directly affect the density of fog droplets in the airflow, which subsequently affects the effectiveness of fog collection. An increase in the sample distance from the humidifier and an expansion of the spray area of the humidifier result in smaller droplet diameters reaching the surface of the fog collector and a decrease in droplet density. From this analysis, it becomes apparent that temperature has minimal impact on the performance of biomimetic fog collectors tested in laboratories due to the use of commercial humidifiers typically employed in high-humidity conditions during testing. Temperature is merely noted as an objective environmental condition, primarily at room temperature.

Experimental conditions and environmental parameters reported in the current literature vary significantly, making it difficult to compare the overall performance of these fog collectors [63]. SWP (mg cm^{-2} h^{-1}) is commonly used in literature as a measure of single fog collection. The fog collection efficiency of the fog collector is defined as

$$\eta_H = M_H / M_F \tag{1.16}$$

Thereafter, M_H represents the amount of fog harvested by the device and M_F represents the overall amount of fog permeating through the collector. Attention is drawn to the discrepancy in environmental conditions under which bioinspired fog collection tests have been conducted across various literature sources, making it challenging to directly compare their collection efficiencies. To address this issue, we include here two key parameters that influence the assessment of bioinspired fog collection performance (i.e. SWP and fog collection efficiency). Taking into account environmental factors that can significantly impact these metrics,

$$\mathrm{SWP} = f(U) * f(\mathrm{RH}) * f(x). \tag{1.17}$$

Specifically, $f(U)$ represents the function describing the velocity of fog droplets, $f(\mathrm{RH})$ represents the humidity condition (which equates to the effect on the flow rate of fog), and $f(\mathrm{L})$ refers to the distance condition between the surface of the fog collector and the humidifier.

References

1 Kummu, M., Guillaume, J.H.A., de Moel, H. et al. (2016). *Scientific Reports* 6: 38495.
2 Liu, J., Yang, H., Gosling, S.N. et al. (2017). *Earth's Future* 5: 545.
3 Alsdorf, D.E., Rodríguez, E., and Lettenmaier, D.P. (2007). *Reviews of Geophysics* 45.
4 Boretti, A. and Rosa, L. (2019). *npj Clean Water* 2: 15.
5 He, C., Liu, Z., Wu, J. et al. (2021). *Nature Communications* 12: 4667.
6 Liu, Z., Ying, J., He, C. et al. (2024). *Landscape Ecology* 39: 10.
7 Thimmappa, R., Gautam, M., Bhat, Z.M. et al. (2021). *Cell Reports Physical Science* 2: 100627.
8 Wang, H. (2018). *Nature Nanotechnology* 13: 273.
9 Liu, Z., Wu, B., Zhu, B. et al. (2019). *Advanced Functional Materials* 29: 1905485.
10 LaPotin, A., Kim, H., Rao, S.R., and Wang, E.N. (2019). *Accounts of Chemical Research* 52: 1588.
11 Ejeian, M. and Wang, R.Z. (2021). *Joule* 5: 1678.
12 Tu, Y., Wang, R., Zhang, Y., and Wang, J. (2018). *Joule* 2: 1452.
13 Guo, J., Huang, W., Guo, Z., and Liu, W. (2022). *Nano Letters* 22: 3104.
14 Wang, W., Pan, Q., Xing, Z. et al. (2022). *Water Research* 211: 118029.
15 Rao, A.K., Fix, A.J., Yang, Y.C., and Warsinger, D.M. (2022). *Energy & Environmental Science* 15: 4025.
16 Rajaram, M., Heng, X., Oza, M., and Luo, C. (2016). *Colloids and Surfaces A: Physicochemical and Engineering Aspects* 508: 218.
17 Shi, W., Anderson, M.J., Tulkoff, J.B. et al. (2018). *ACS Applied Materials & Interfaces* 10: 11979.
18 Wang, X., Guo, Z., and Liu, W. (2023). *Advanced Materials Interfaces* 10: 2202123.
19 Lei, J. and Guo, Z. (2020). *Nanoscale* 12: 6921.
20 Rivera, J.d.D. (2011). *Atmospheric Research* 102: 335.
21 Wenzel, R.N. (1949). *The Journal of Physical and Colloid Chefogry* 53: 1466.
22 Zhu, H., Guo, Z., and Liu, W. (2016). *Chemical Communications* 52: 3863.
23 Si, Y. and Dong, Z. (2020). *Langmuir* 36: 667.
24 Zhang, H., Wang, F., and Guo, Z. (2024). *Advances in Colloid and Interface Science* 325: 103097.
25 Schemenauer, R.S., Fuenzalida, H., and Cereceda, P. (1988). *Bulletin of the American Meteorological Society* 69: 138.
26 Schemenauer, R.S. and Cereceda, P. (1991). *Ambio* 20: 303.
27 Parker, A.R. and Lawrence, C.R. (2001). *Nature* 414: 33.

28 Seely, M.K. and Hamilton, W.J. (1976). *Science* 193: 484.
29 Gao, Y., Wang, J., Xia, W. et al. (2018). *ACS Sustainable Chefogry & Engineering* 6: 7216.
30 Xu, C., Feng, R., Song, F. et al. (2018). *ACS Sustainable Chefogry & Engineering* 6: 14679.
31 Knapczyk-Korczak, J., Ura, D.P., Gajek, M. et al. (2020). *ACS Applied Materials & Interfaces* 12: 1665.
32 Sarkar, D., Mahapatra, A., Som, A. et al. (2018). *Advanced Materials Interfaces* 5: 1800667.
33 Bai, H., Wang, L., Ju, J. et al. (2014). *Advanced Materials* 26: 5025.
34 Chen, W. and Guo, Z. (2019). *Nanoscale* 11: 15448.
35 Rykaczewski, K., Jordan, J.S., Linder, R. et al. (2016). *Langmuir* 32: 9335.
36 Cao, M., Ju, J., Li, K. et al. (2014). *Advanced Functional Materials* 24: 3235.
37 Li, X., Yang, Y., Liu, L. et al. (2020). *Advanced Materials Interfaces* 7: 1901752.
38 Chen, D., Li, J., Zhao, J. et al. (2018). *Journal of Colloid and Interface Science* 530: 274.
39 Chen, H., Ran, T., Gan, Y. et al. (2018). *Nature Materials* 17: 935.
40 Dai, X., Sun, N., Nielsen, S.O. et al. *Science Advances* 4: eaaq0919.
41 Pan, Z., Pitt, W.G., Zhang, Y. et al. (2016). *Nature Plants* 2: 16076.
42 Nishimura, R., Hyodo, K., Mayama, H. et al. (2019). *Communications Chefogry* 2: 90.
43 Yang, H., Zhu, H., Hendrix, M.M.R.M. et al. (2013). *Advanced Materials* 25: 1150.
44 Ni, F., Xiao, P., Qiu, N. et al. (2020). *Nano Energy* 68: 104311.
45 Xing, C., Huang, D., Chen, S. et al. (2019). *Advanced Science* 6: 1900531.
46 Li, R., Shi, Y., Shi, L. et al. (2018). *Environmental Science & Technology* 52: 5398.
47 Ni, F., Xiao, P., Zhang, C. et al. (2019). *ACS Applied Materials & Interfaces* 11: 15498.
48 Wang, M., Sun, T., Wan, D. et al. (2021). *Nano Energy* 80: 105569.
49 Li, R., Shi, Y., Alsaedi, M. et al. (2018). *Environmental Science & Technology* 52: 11367.
50 Xu, J., Li, T., Chao, J. et al. (2020). *Angewandte Chemie International Edition* 59: 5202.
51 Gou, X. and Guo, Z. (2020). *Langmuir* 36: 64.
52 Yang, X., Liu, X., Lu, Y. et al. (2016). *The Journal of Physical Chefogry C* 120: 7233.
53 Feng, J., Zhong, L., and Guo, Z. (2020). *Chemical Engineering Journal* 388: 124283.
54 Wang, B., Zhang, Y., Liang, W. et al. (2014). *Journal of Materials Chefogry A* 2: 7845.
55 Zhang, L., Wu, J., Hedhili, M.N. et al. (2015). *Journal of Materials Chefogry A* 3: 2844.
56 Ping, Z., Sun, Q., Yi, J. et al. (2021). *ACS Applied Materials & Interfaces* 13: 49556.
57 Zhao, J., Deng, Y., Dai, M. et al. (2022). *Journal of Water Process Engineering* 46.
58 Liu, Y.F., Yang, N., Li, X. et al. (2020). *Small* 16.

59 Tian, X.L., Chen, Y., Zheng, Y.M. et al. (2011). *Advanced Materials* 23: 5486.

60 Hou, Y.P., Chen, Y., Xue, Y. et al. (2012). *Soft Matter* 8: 11236.

61 Tang, X., Huang, J.X., Guo, Z.G., and Liu, W.M. (2021). *Journal of Colloid and Interface Science* 604: 526.

62 Peng, Y., He, Y.X., Yang, S. et al. (2015). *Advanced Functional Materials* 25: 5967.

63 Yu, Z.H., Zhu, T.X., Zhang, J.C. et al. (2022). *Advanced Functional Materials* 32.

64 Zhou, H., Jing, X.S., and Guo, Z.G. (2020). *Journal of Colloid and Interface Science* 561: 730.

65 Zhou, H., Zhang, M.X., Li, C. et al. (2018). *Small* 14.

66 Zhou, H., Jing, X.S., Li, S.P., and Guo, Z.G. (2021). *Chemical Engineering Journal* 417.

67 Zhong, L.S., Zhang, R.C., Li, J. et al. (2018). *Langmuir* 34: 15259.

68 Ju, J., Yao, X., Yang, S. et al. (2014). *Advanced Functional Materials* 24: 6933.

69 Bagheri, F. (2021). *Water Resources and Industry* 25.

70 Gido, B., Friedler, E., and Broday, D.M. (2016). *Atmospheric Research* 182: 156.

71 Bussmann, M., Mostaghimi, J., and Chandra, S. (1999). *Physics of Fluids* 11: 1406.

72 Zhong, L.S., Zhu, H., Wu, Y., and Guo, Z.G. (2018). *Journal of Colloid and Interface Science* 525: 234.